Nanoscale alloys and core-shell materials: Model predictions of the nanostructure and mechanical properties

E. E. Zhurkin,[1] T. Van Hoof,[2] and M. Hou[2,*]

[1]*Department of Experimental Nuclear Physics, Physical and Mechanical Faculty, K-89, St. Petersburg State Polytechnical University, 29 Polytekhnicheskaya Strasse, 195251 St. Petersburg, Russia*

[2]*Physique des Solides Irradiés et des Nanostructures CP234, Université Libre de Bruxelles, Bd Du Triomphe, B-1050 Bruxelles, Belgium*

(Received 29 December 2006; revised manuscript received 10 March 2007; published 4 June 2007)

Atomic scale modeling methods are used to investigate the relationship between the properties of clusters of nanometer size and the materials that can be synthesized by assembling them. The examples of very different bimetallic systems are used. The first one is the Ni_3Al ordered alloy and the second is the AgCo core-shell system. While the Ni_3Al cluster assembled materials modeling is already reported in our previous work, here we focus on the prediction of new materials synthesized by low energy deposition and accumulation of AgCo clusters. It is found that the core-shell structure is preserved by deposition with energies typical of low energy cluster beam deposition, although deposition may induce substantial cluster deformation. In contrast with Ni_3Al deposited cluster assemblies, no grain boundary between clusters survives deposition and the silver shells merge into a noncrystalline system with a layered structure, in which the fcc Co grains are embedded. To our knowledge, such a material has not yet been synthesized experimentally. Mechanical properties are discussed by confronting the behaviors of Ni_3Al and AgCo under the effect of a uniaxial load. To this end, a molecular dynamics scheme is established in view of circumventing rate effects inherent to short term modeling and thereby allowing to examine large plastic deformation mechanisms. Although the mechanisms are different, large plastic deformations are found to improve the elastic properties of both the Ni_3Al and AgCo systems by stabilizing their nanostructure. Beyond this improvement, when the load is further increased, the Ni_3Al system displays reduced ductility while the AgCo system is superplastic. The superplasticity is explained by the fact that the layered structure of the Ag system is not modified by the deformation. Some coalescence of the Co grains is identified as a geometrical effect and is suggested to be a limiting factor to superplasticity.

DOI: 10.1103/PhysRevB.75.224102 PACS number(s): 61.43.Bn, 61.46.Hk, 61.66.Dk, 62.20.Fe

I. INTRODUCTION

The science of nanostructured materials (NSMs) spans over several scales bounded on the one hand by the atomic scale and on the other by the macroscopic scale and characteristic times from the atomic lattice vibration to the lifetime of a device in service. The main question linking these scales together is how to identify the relationship between nanoscopic and macroscopic properties. For instance, in order to understand the causality between texture at the nanometer scale and the macroscopic mechanical behavior, the relationship between properties of the building blocks and of the macroscopic material needs to be clarified. This question forms the context of the present report, with emphasis on nanostructured materials formed by two different metals.

The literature about mechanical deformation mechanisms in nanostructured materials is abundant and significant fundamental progress is motivated by potential significance for engineering applications. Mechanical properties specific to the nanoscale were pointed by the violation of the Hall-Petch hardening mechanism[1,2] whereby the resistance to plastic flow is determined by dislocation pile up. This process breaks down at the nanoscale at which no dislocation pile up takes place.[3] Evidence was found for superplasticity at low temperature in nanostructured metals[4] which mechanisms in the absence of dislocations activity are not yet well understood. Considering the high difficulty to evidence nanoscale mechanisms experimentally, atomic scale modeling is particularly attractive and several groups used computer simulation with the aim to set up comprehensive models. Particular attention was paid to the interplay between dislocation and grain boundary mechanisms.[5–12] Model materials used in these studies were mainly fcc, sometimes bcc elemental metals, and the deformation mechanisms at work in nanostructured ordered cubic alloys were found to be qualitatively similar.[13] There is a wide variety of possible grain boundaries in materials[14] and deformation mechanisms involving them may be expected to depend on their structure at the atomic scale. Modeling suggested the importance of small open volumes containing no more than a few vacancies on the nucleation and emission of dislocations.[9] Voids can be much larger, however, and even of the same size as the nanograins themselves when the nanostructured material is synthesized by assembling clusters.[15] Simulated NSMs may be constructed in different ways, eventually mimicking experimental one and two step preparation methods. The former (e.g., electrodeposition or severe plastic deformation) give rise to dense compact materials. The atomic scale structure of such materials is modeled, for instance, by Voronoi constructions.[16] We here focus on the latter [e.g., using inert gas condensation followed by compaction or nanocluster synthesis followed by low energy cluster beam deposition (LECBD)]. Such cluster assembled materials (CAMs) invariably contain voids and may therefore have significantly lower average densities than polycrystals, single crystals, and NSMs synthesized by a one step method. The accumulation

of energetic metallic clusters on a solid substrate was modeled in Ref. 17. Realistic atomic scale modeling of cluster assembled layers is discussed in Refs. 15 and 18. This way, a route was opened for a coherent sequence of models from the cluster to the CAM, the same characterization method of their properties, and the relationship between them.

Metallic nanoparticles with diameters typically less than 10 nm attract much interest because of their specific structural, chemical, optical, magnetic, and electronic properties. Many of them are reviewed in Refs. 19–22. These properties often scale with their size.[23] Specially stable structures of well-defined cluster sizes are known and appear as "magic numbers" in mass spectra[24] associated with electronic shells closure as the smallest ones are concerned with close packed geometries in larger clusters.[24–29] Such particles display original physical properties that can be controlled by monitoring the cluster composition and that might be of technological interest. One example is magnetic structures obtained in arrays of clusters deposited on a surface[30–32] specific to the clusters themselves, but also to their interaction with their environment, as reviewed in Ref. 33. In a material made by assembling clusters, the environment of each individual is formed by other clusters, the interface with a substrate, and free surfaces. The nanostructure formed in such a way depends on the assembling conditions. For instance, inert gas condensation followed by compaction[34,35] leads to materials with some open volumes and with a density reduced by a few percent as compared to a polycrystalline material of the same composition. LECBD allows depositing clusters on a substrate from a mass selected beam of clusters with supersonic velocities, representing typically kinetic energies of a fraction of an eV per atom.[32] Such films were observed where clusters may keep their identity,[15,18] in which case they are separated by pores with characteristic size of the same order as the cluster diameters. Atomic scale modeling predicts this nanostructure to be sensitive to the precise kinetic energy of the clusters in the beam.[15] For this reason, understanding the relationship between the film morphology and the relevant cluster properties before deposition requires characterizing the detail of the cluster evolution during deposition. This is the line followed in our previous study of Ni_3Al nanostructured films[36–38] and along which we proceed in what follows.

In Sec. II, the modeling of Ni_3Al CAMs is briefly surveyed as well as of AgCo clusters used for synthesizing AgCo core-shell materials. Section III shortly reviews the modeling methods used, based on molecular dynamics (MD) and Metropolis Monte Carlo (MMC) algorithms. The tools used for characterizing clusters and CAMs in a consistent way are listed in Sec. IV. Suitable references are given in the two latter sections for more detailed discussion. Section V is devoted to the layers formed by deposition of core-shell AgCo clusters and the relationship between the clusters and the layers properties. Section VI is devoted to the modeling of the mechanical properties of nanoalloys and core-shell CAMs with a focus on large deformations. A conclusion is presented in Sec. VII.

II. Ni_3Al AND AgCo CORE-SHELL CAM

As far as Ni_3Al clusters of realistic sizes are concerned, equilibrium structural phases were first identified by means of Metropolis Monte Carlo (MMC) simulations and found to be the same as for the bulk material.[36] In particular, the $L1_2$ structure known in bulk Ni_3Al is retrieved in clusters formed by 200 atoms and more. This ordered phase keeps stable at all temperatures below the melting point. Surface segregation of Al was found possible, not exceeding 10%. The ordered cluster cores are in equilibrium with disordered outer shells. The deposition of a cluster on a crystalline surface was modeled by molecular dynamics (MD). The impact of the clusters with supersonic velocities (a fraction of an eV per atom) combined with thermal activation was found to result in a limited decrease of short range order in the cluster correlated with an increase of epitaxial accommodation with the substrate. The accumulation of clusters to form a cluster assembled film was studied in a third step by MD and it was found that as soon as one cluster monolayer is formed, no epitaxial relationship between further deposited clusters and the substrate is to be expected. The morphology of the Ni_3Al cluster assembled film obtained is nanoporous and not very dependent on the deposition energy. MMC simulations on the deposited film indicate no significant change in the segregation state at cluster interfaces. Hence, this is a case where a cluster assembled material retains pretty well the memory of the structural properties of the clusters before assembling. In a fourth step, mechanical properties of this material were studied, using MD again.[13,39] The hydrostatic pressure in isolated clusters is of the order of 2 GPa, as found previously in elemental clusters of the same size[40] (no more than a few nanometers diameter) balanced by a surface tensile stress. Al is overpressurized (to about 5 GPa) and Ni underpressurized (to about −1 GPa). The difference in mean atomic pressures is increased by the deposition on a surface and the deposited film is characterized by a huge heterogeneity in the distribution of local stress. The Young modulus of the nanostructured system is reduced as compared to the bulk and a temperature dependent yield strength is found. In the plastic regime, deformation is characterized mainly by the increase of open volumes, some grain sliding, and a limited dislocation activity, even in clusters as small as 2 nm diameter.

Peculiar properties may also be speculated in materials made of clusters which composition does not exist at the macroscopic scale. This is the case of AgCo clusters which components are not miscible in the bulk, but are currently synthesized with adequate cluster sources.[41,42] Depending upon their size and their composition, the spatial arrangement of Ag and Co atoms in clusters may consist in a Co core surrounded by a Ag shell. Such arrangements were found experimentally[41,43] and studied theoretically.[44–47] Low and high limits to the Co concentration were found for the occurrence of AgCo core-shell structures. These limits were explained in terms of a competition between binding and stress, and of a consequence of the wetting of the Co cores by Ag.

When the Ag shell is shallow enough, the strain induced by the lattice mismatch at the Ag/Co interface is such high that the Ag shell does not keep its crystalline structure and the possible thickness of this noncrystalline shell increases with temperature. Typically, a cluster containing about 3000 atoms may include four noncrystalline layers at room tem-

perature. This feature indicates that, if such clusters can be assembled into a material, this one might be formed by small Co grains embedded in noncrystalline Ag shells, and properties specific to this lack of crystallinity could be anticipated.

Following the same line as for the Ni_3Al alloy nanomaterial, the deposition of single AgCo clusters on a surface was already studied in detail,[48] showing that the consequences of the impact are not very dependent on the conditions of incidence and that, although significant atomic rearrangements may occur, the clusters keep their core-shell structure after deposition and first neighbor contacts between Co grains are exceptional. Because of their lack of crystallinity constrained by the Co cores, the Ag shells only undergo limited epitaxial accommodation with the Ag substrate and, as a result of negligible penetration, accumulating clusters on the surface has the consequence of a sharp interface between the substrate and the core-shell cluster layer.[49]

III. MODELING METHODS

Clusters used for LECBD are of ideal size to be studied at the atomic scale, as well as the solid films formed by their accumulation. Indeed, realistic clusters do not contain more than a few hundred to a few thousand atoms each and less than one hundred thousand atoms is generally sufficient to model a thin film and its surface realistically.[17]

Different MD schemes are here employed, based on the same interaction model between the atoms. The force field in the Ni_3Al system is derived semiempirically from the second moment tight binding approximation[50–53] and the potential parameters are those suggested in Ref. 54. Atomic interactions in the AgCo system are described by the embedded atom model (EAM)[55] with the functional of the electronic density suggested in Refs. 56 and 57 and assessed for the AgCo system in Ref. 58. Clusters at equilibrium before deposition are modeled by MMC (Ref. 59) in the (NPT) canonical ensemble discussed in Refs. 36 and 47.

Nanostructured materials are characterized by deep inhomogeneities and studying their evolution requires one to account for the dynamics of the macroscopic deformation of the simulation box, at constant external pressure and temperature. This is achieved in the canonical ensemble according to the constrained MD scheme introduced by Parrinello and Rahman[60,61] using a Nosé thermostat.[62]

One of the essential ingredients of the Parrinello-Rahman Lagrangian is the stress tensor of which appropriate components may be frozen in order to model an external constraint. This is the method used below in order to study the mechanical response of model samples to an external uniaxial load.

When a cluster slows down on a surface, it is necessary to account for the dynamic exchange of energy between the ionic and the electronic systems, which is responsible for a large part of the energy dissipation after the cluster impact. In the present work the approach suggested in Ref. 63 is used, which accounts for the electron-phonon coupling on the basis of the Sommerfeld theory of metals.[15]

Conventional MD approaches are unable to model large plastic deformations and we propose a scheme to circumvent this deficiency. The problem is as follows.

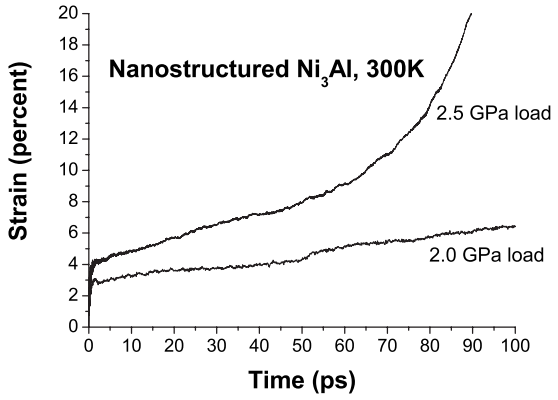

FIG. 1. Time dependence of strain under uniaxial stress. Strain is represented versus time during 100 ps for the Ni_3Al cluster assembled material at 300 K in the case of two different loads: one where strain increases linearly with time and one where the strain rate diverges.

Figure 1 shows the strain as a function of time in MD simulations of a Ni_3Al CAM subjected to different constant uniaxial loads at constant temperature. With the lowest stress shown, the strain increases linearly with time. This is the plastic regime discussed in detail in Ref. 13. Increasing the load results in an increase of the strain rate and, when this one is too high, decohesion of the material results. This situation, typical to MD simulations, is discussed in Ref. 64. Strains involved in Fig. 1 increase by more than 2% within 100 ps, which represents a strain rate higher then 5×10^8 s^{-1}, about 10 orders of magnitude larger than in real standard tensile deformation tests. Thus, the computer experiments as described in Fig. 1 only capture deformation way out of the thermodynamic equilibrium to which real experiments are closer. On the other hand, the time scales involved in a real experiment involving slow deformation are also way out of the range attainable in standard MD simulations. It is, however, possible to design a procedure whereby the system under load is constraint closer to equilibrium while the computer times involved remain practical. The method adopted here consists in sequences of cycles of alternate isothermal loading and relaxation to thermal equilibrium in the absence of an external stress. The shorter the loading time, the closest to equilibrium state the system remains. In order to avoid the divergence of the strain rate, it is possible to apply a load during a time interval short enough that the strain rate is close to constant, though sufficient to induce a limited permanent deformation. The situation is described in Fig. 2(a). A load of 2.7 GPa is applied during 30 ps at 300 K to a nanostructured Ni_3Al sample synthesized by CAM deposition with 0.25 eV per atom. For the sake of efficiency, modeling relaxation toward thermal equilibrium is then achieved in two steps. The load being released, the system is first quenched to 0 K by time steps of 2 fs during 5 ps in order to let it quickly approach to a local minimal energy configuration. It is then brought to thermal equilibrium at 300 K again before the cycle is repeated. This thermalization here lasts 15 ps. According to the successive steps of the deformation cycle, Fig. 2(b) shows that the density of the sample decreases during loading, increases as a consequence

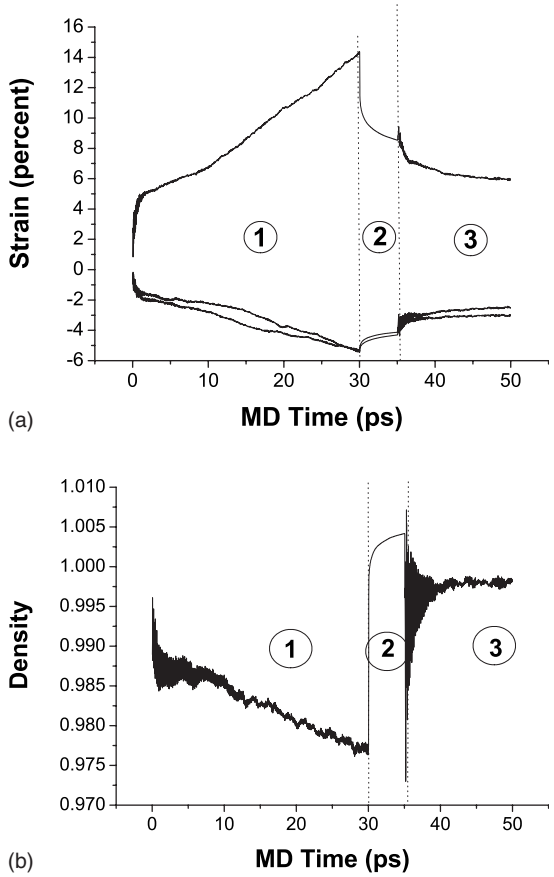

FIG. 2. One deformation cycle of the Ni_3Al sample. A uniaxial load of 2.7 GPa is applied to the CAM Ni_3Al sample at 300 K during 30 ps (region 1). The load is then released and the sample is quenched at 0 K for 5 ps (region 2). It is then brought of thermal equilibrium by an unconstraint MD run of 15 ps (region 3). (a) Strain (the upper curve shows the strain in the direction of the load and the lower ones the strain in two orthogonal directions in the plane perpendicular to the loading direction). (b) Density, as relative to the density of the undeformed sample. The same convention is used in Figs. 13 and 16. It must be noted that the MD time does not correspond to the time in a real experiment. The quenching and thermalization steps (regions 2 and 3) are indeed applied for artificially bringing the system back to equilibrium after deformation with a high strain rate for a short time.

of quenching at 0 K, and levels off at an equilibrium value during the following free evolution at 300 K. In several cases, the loading time in a cycle was modified and it was checked that the deformation on a few cycles was only dependent on the total loading time and not significantly on the time elapsed in each cycle. In such conditions, the loading time in each cycle was considered satisfactorily short.

Deformation mechanisms induced by an external stress may be regarded as twofold. On the one hand, there is the Newtonian response which determines the trajectories of the atoms and it is fully accounted for by the first part of the deformation cycle described in Fig. 2(a). On the other hand, there are the thermally activated processes that may occur on any time scale, including macroscopic, and are thus only partly accounted for by the third part of the cycle in Fig. 2(a). Hence, the nanostructural evolution of large plastic deformation under stress depicted in Sec. VI avoid strain rate divergence inherent to conventional MD but is limited to short term contributions. Therefore, the stochastically induced contributions arising during the successive thermal equilibrium phases considered are underestimated. In principle, alternative schemes may conveniently be applied to the thermal equilibrium phase of the cycles, such as hyperdynamics,[65] temperature accelerated dynamic schemes,[66] or any other scheme allowing for handling rare events.[67] These represent a further level of sophistication of the present approach considered for later studies.

IV. CHARACTERIZATION TOOLS

Several parameters already described in Ref. 49 are used for characterizing the nanostructured layer. The same definition of a pair distribution function (pdf) as in Ref. 22 is used to characterize short range order in the clusters. It is used for discussing crystallinity.

The nanostructure is also characterized by the first neighbor coordination of the atoms. In practice, its estimate is a little ambiguous in the case of high strain fields. Coordination is measured for atom pairs with separation distances smaller than a cutoff distance. The definition of this cutoff distance causes no problem in the Ni_3Al systems where the first and second neighbor peaks in the pdfs are always well separated. The case of AgCo is more ambiguous, because of the occurrence of large relaxations. It is taken equal to 0.33 nm, which is close to the minimum between the first and second neighbor peaks of the pair distribution functions in crystalline silver. This value is empirically found reasonable, although it is not strictly correct. Nevertheless, it suffices to distinguish internal surface atoms from atoms in grain cores on the basis of a coordination number criterion. In the nanostructure, atoms with estimated coordination numbers less than or equal to 9 are considered as surface atoms.

It is also desired to estimate the extent to which the initial core-shell structure of the AgCo clusters is degraded by the deposition and the deformation processes. To this purpose, the connectivity between Co cores is analyzed. This is done by counting the number of Co first neighbor pairs belonging to different initial clusters.

Finally, the deformation of clusters is estimated by an aspect ratio which can be estimated for each species forming the clusters. To this purpose, two ellipsoids are associated with each cluster, using a component analysis method.[68] The eigenvector associated with the largest eigenvalue α of the covariance matrix has the direction maximizing the variance of the position distribution and this eigenvalue is the variance of the position distribution projected onto this eigenvector. The eigenvector associated with the smallest eigenvalue, γ, has the direction minimizing the variance in a plane orthogonal to the first. The aspect ratio is here defined by $\frac{\alpha}{\gamma} - 1$ which represents the offset from sphericity.

V. AgCo CLUSTERS, CLUSTER DEPOSITION, AND CLUSTER ASSEMBLIES

A. Clusters

The sequence to set up the initial slowing down conditions is as follows. Initial clusters are prepared as described

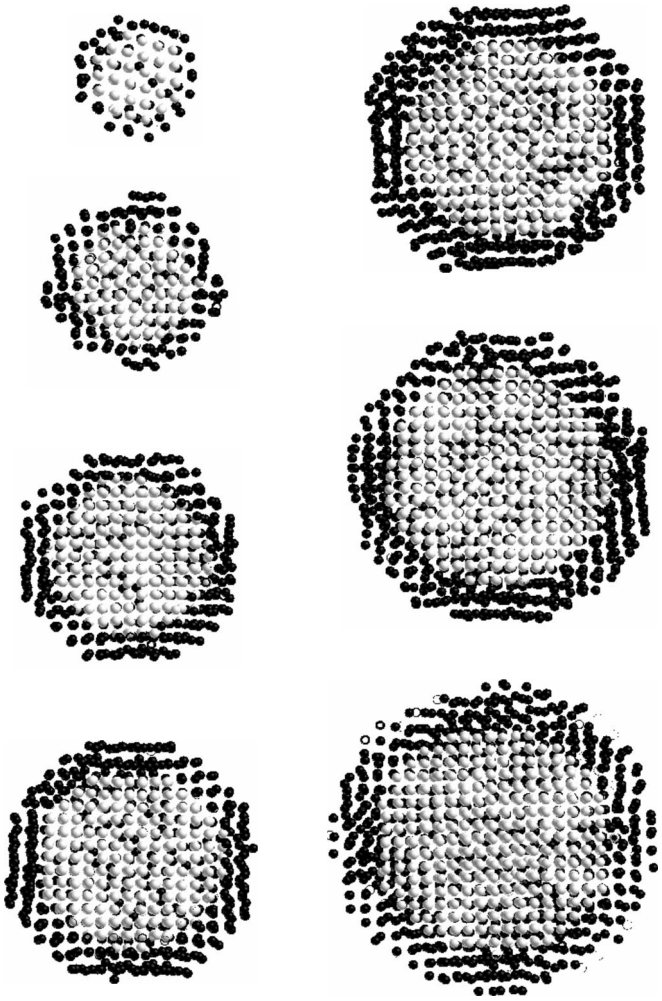

FIG. 3. Equilibrium cluster configurations at 300 K before deposition. Cuts are shown in clusters containing 200, 500, 1000, 1500, 2000, 2500, and 3000 atoms. Dark and light spheres represent Ag and Co atoms, respectively.

in Ref. 22. They are obtained by cutting spheres with given radii in a perfect fcc box where Ag and Co atoms may be distributed at random. MMC sampling in the (NPT) canonical ensemble is then used to predict the equilibrium atomic configuration of each cluster at room temperature. Second, the velocities in the center of mass system of the cluster are determined by MD. To this purpose, atoms are first slightly and randomly displaced from their static equilibrium positions. Velocities are then gradually rescaled until the system finds a thermal equilibrium state at the desired temperature.

Equilibrium configurations at 300 K of the AgCo clusters used in what follows are shown in Fig. 3 and all display, as expected, a core-shell structure. Pair distribution functions for Ag and Co are given in Fig. 4 for the largest one (3000 atoms). They clearly show that the Co core is crystalline with an fcc structure while, because of the Ag/Co lattice mismatch, silver is not, as attested by the absence of a second neighbor peak near 0.4 nm. It is also not liquid, as attested by the larger distance structure in the pdf, which is the signature of the Ag layered structure seen in Fig. 3 and imposed by the crystalline Co core. The synthesis of self-standing

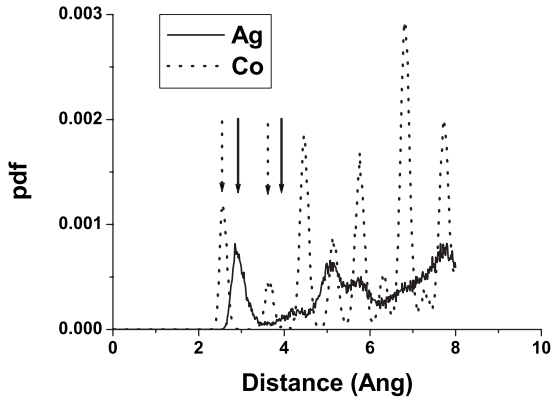

FIG. 4. Pair distribution functions estimated for Co (dotted line) and Ag (solid line) in the $Ag_{1500}Co_{1500}$ cluster at 300 K. Vertical dotted and solid arrows show the expected positions of first and second neighbor peaks in Co and Ag, respectively. The Ag second neighbor peak is missing.

amorphous Ag nanoparticles is reported in the literature[69] that were found metastable and to crystallize at 640 K. In our model core-shell particles, as shown in Ref. 22, the stability of the layered noncrystalline structure is warranted by the Co cores and its thickness is an increasing rather decreasing function of temperature. The consequences of this layering will be discussed further in the following sections.

B. Cluster deposition

In a previous work,[15] the deposition of gold clusters on Au(111) was modeled by molecular dynamics (MD), using similar cluster size distributions and incident kinetic energies as in real LECBD experiments.[18] The problem with MD is that the method does not allow modeling the long term evolution of a system and, among others, cluster diffusion on a substrate surface is thus hardly depicted. However, it was observed experimentally, using STM measurements that gold clusters deposited on a gold (111) surface are not diffusing.[18] Their size distribution measured after deposition was also found the same as before deposition. Hence, the film growth takes place as deposition proceeds by stacking of clusters without any detectable coalescence. In such conditions, the modeled film morphology agreed very well with STM observations on real samples.

For modeling deposition, a cluster was initially positioned at a distance from the substrate, which is just sufficient for cluster atoms closest to the surface to interact with surface atoms. Before starting the dynamics of the cluster-surface interaction, the cluster was rotated at random around its center-of-mass and directional correlations between the cluster and the surface initial orientations were thereby avoided. The impact (translation) energies of the clusters were selected as 0.1, 0.25, and 0.5 eV/at. This way, the energy range typical of LECBD was covered.[32] The evolution of the system was followed during 100 ps before the next cluster was deposited. This period of time is longer than the impact itself (a few ps) as well as than the electron-phonon characteristic coupling time in silver at room temperature (22.5 ps according to the Sommerfeld theory of metals[15]). It is assumed that

it reached thermodynamic equilibrium before the impact of another cluster in its vicinity. When an energetic cluster is impacting on a solid surface, an elastic shock wave might eventually be generated, which needs to be damped in a finite simulation box in order to avoid possible artifacts. Since slowing down energies in the LECBD regime are low, the problem is not crucial. In the present simulation context, an additional coupling force to the electron thermostat was applied at the bottom of the substrate, with a very short time constant. This force was switched off shortly after a time interval long enough for a sound wave to cross the whole substrate thickness. The box size was checked to be large enough to prevent any significant size effect on the dynamics of deposition.

C. Cluster assemblies

1. Modeling conditions

The substrate is a Ag (001) single crystal box to which periodic boundary conditions were applied in the [100] and the [010] directions. The surface is a square with 24 cell edge units side length and the thickness is 18 lattice units. Before the slowing down was started, the substrate was set to thermal equilibrium at 300 K. The six clusters shown in Fig. 3 have diameters ranging from 2 to 4.5 nm. They were sampled at random for slowing down, according to a typical experimental size distribution, close to log-normal.[70] The evolution of the simulation box after one cluster impact was not found significant after a 100 ps delay. Up to 80 clusters were accumulated for each impact energy, which represents a time of the order of 10 ns to form a layer. The same periodic boundary conditions were applied in this layer as to the substrate.

For the modeling of this nanostructured layer as well as of mechanical deformation, parallel versions of the MD codes designed for distributed memory architectures were useful. They were ran with the MPI software using 27 nodes equipped with one 2.8 GHz processor each and interconnected with a Gigabit network.

2. The overall nanostructure

The nanostructured layers obtained with 0.1, 0.25, and 0.5 eV/at. are depicted in Fig. 5. In the first column, Ag and Co atoms are differentiated. Whatever the energy, the core-shell structure appears to a large extent preserved. Its degradation is discussed in more detail in the next section. To our knowledge, such a "core-shell material" is not yet synthesized experimentally. In the case of the lowest deposition energy, many open volumes characterize the layers that are connected and form pores. This is evidenced in Fig. 5(b) (second column) where only atoms with coordination numbers less than 9 are represented. In the case of 0.1 eV/at. deposition, the diameter of the pores is of the order of the diameter of the largest cluster and the area of the internal surfaces is particularly large. Open volumes are much smaller with higher deposition energy and internal surfaces are practically nonexistent in the case of 0.5 eV/at. deposition. No more than one percent low coordination Co is found. A detailed analysis of the configurations shows that most of them belong to the Ag-Co core-shell internal interfaces and those at interfaces between clusters are infrequent.

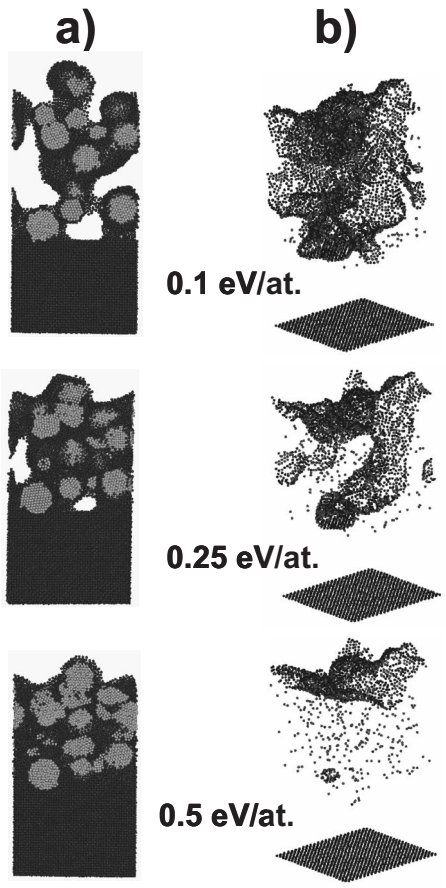

FIG. 5. Final atomic configurations obtained with 0.1, 0.25, and 0.5 eV per atom energy deposition. A slab of 2 nm thick is represented in column (a). In column (b), only the atoms with coordination number $Z \leqslant 9$ are represented, mapping both internal and external surfaces.

We now turn to the examination of the crystallinity of the nanostructured layer and we start with the Ag subsystem. Figure 6 shows Ag pair distribution functions in slabs parallel to the substrate surface. Slabs are 0.4 nm thick. The pdfs are shown in the two first substrate layers adjacent to the interface with the cluster layer and in five successive slabs in the latter. In the substrate, the pdf is characteristic of the fcc structure. The situation is totally different in the nanostructured layer. For all deposition energies, the second neighbor peak in the interfacial slab is strongly attenuated as compared to the substrate and it vanishes as the distance from the interface increases. Hence, the thickness of the nanostructured layer displaying a crystalline character in the Ag subsystem is shallow and decreases with increasing deposition energy. It is no more than four lattice spacings for 0.1 eV/at. and two lattice spacings for 0.5 eV/at.

The cobalt cluster cores are not influenced by the deposition and they keep crystalline. Epitaxial accommodation is thus limited to the substrate/nanolayer interface only.[49]

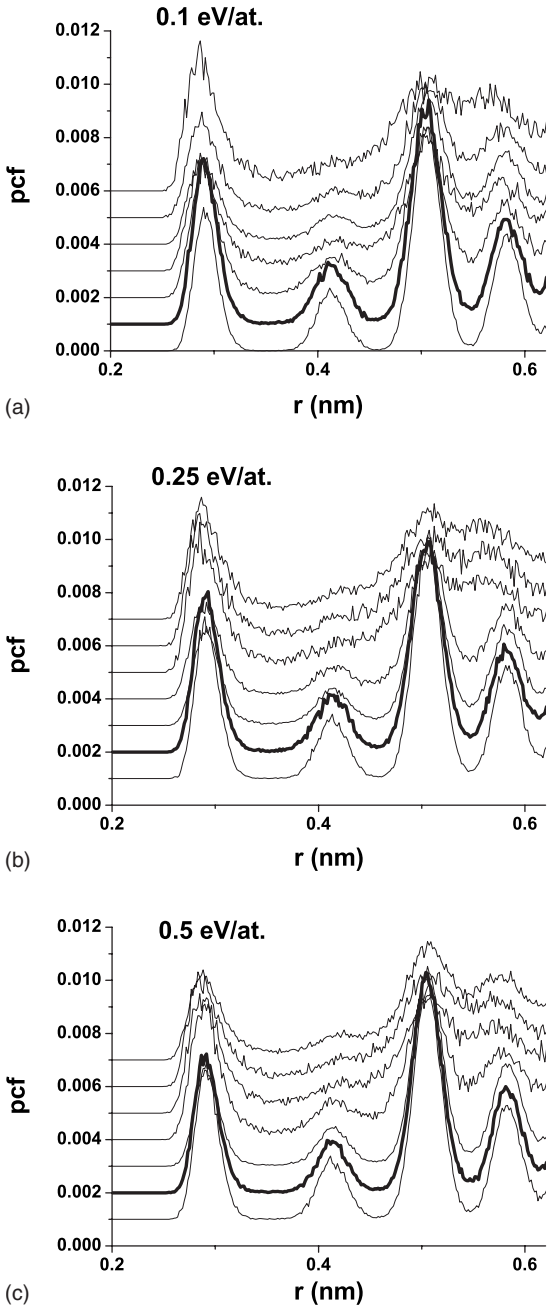

FIG. 6. Ag-Ag pair distribution functions in successive slabs of 0.4 nm starting from 0.8 nm below the substrate surface. The pdfs above the thick line are calculated in the cluster deposited layers. They are given for the three samples with clusters deposited with slowing energies of (a) 0.1 eV/at., (b) 0.25 eV/at., and (c) 0.5 eV/at.

3. The assembled clusters

We now look at the deformation of clusters during the slowing down by means of their aspect ratio. Figure 7 shows the aspect ratio of the silver shells and of the cobalt cores as functions of the cluster size in the three samples. It is displayed just after deposition in order to measure the deformation subsequent to the impact and at the end of the layer synthesis in order to measure the deformation subsequent to the deposition of the next clusters. The comparison of the results for Ag and Co shows that the deformations of the silver shells are always larger than those of the Co cores. As Co is concerned, the aspect ratio increases with the cluster size, showing that largest Co groups are only a little sensitive to the slowing down energy. No clear trend is found in this respect for Ag. There is some variability in the deformation from one cluster to another and the dispersion is increased by the deposition of additional clusters. As Ag is concerned, the standard deviation of the aspect ratio distribution increases with size from 10–30% in the case of 0.5 eV/at. deposition. This is to be correlated with the fact that, in this sample, open volumes are filled. This is caused by the flow of Ag atoms in between Co cores during impact, which is more effective in the largest clusters having the thickest Ag shells.

VI. MECHANICAL PROPERTIES

A. Internal stress distribution in deposited layers

In order to emphasize the importance of the nanostructure on mechanical properties, in what follows, the cases of Ni_3Al and AgCo cluster assembled materials are compared, with a particular focus on large plastic deformations. The Parrinello-Rahman approach is therefore used. Since it requires solving the equations of motion in a reduced coordinate system with periodic boundary conditions, it is inadequate to model external surfaces. Therefore, the samples depicted in the previous section cannot be used as such. As previously done in the case of Ni_3Al,[13] an orthogonal box is cut in the nanostructured layers depicted in Fig. 5 which is then relaxed and brought to thermal equilibrium with a Parrinello-Rahman scheme using periodic boundary conditions. This procedure inevitably induces undesirable stress at the artificial interfaces generated by the periodic boundary conditions. A careful examination of their effect was carried on in the case of Ni_3Al (Ref. 13) and this additional stress was found insignificant as compared to the existing stress at cluster interfaces and in their core, inherent to the nanostructure. The same is found here in the case of the AgCo system as formed by 0.25 and 0.5 eV/at. deposition, although the stress situations in Ni_3Al and AgCo cluster assembled materials are quite different. As the layer formed with 0.1 eV/at. deposition is concerned, the interfacial contacts between clusters are such limited (see Fig. 5) that they do not suffice to warrant the stability of the structure at room temperature. Subsequently, except at lower temperature, detaching the layer from the substrate induces spontaneous sintering and, on the long term, the nanostructure becomes similar to that obtained with 0.25 eV deposition energy.

In Ni_3Al CAM, the high mean pressure in isolated clusters is released, on average, as a consequence of assembling; however, the width of the pressure distribution on the atoms was found fairly increased (typically 5 GPa), revealing highly inhomogeneous internal stress. The same characteristics are found, qualitatively, in the AgCo systems. Average pressures are, however, one order of magnitude lower while the width of their distribution is a factor 2 smaller, being the largest in the Ag subsystem. Typical pressure distributions are shown in Fig. 8. The Ag system is, on average, slightly overpressurized (0.4 GPa) while the Co cores are subjected

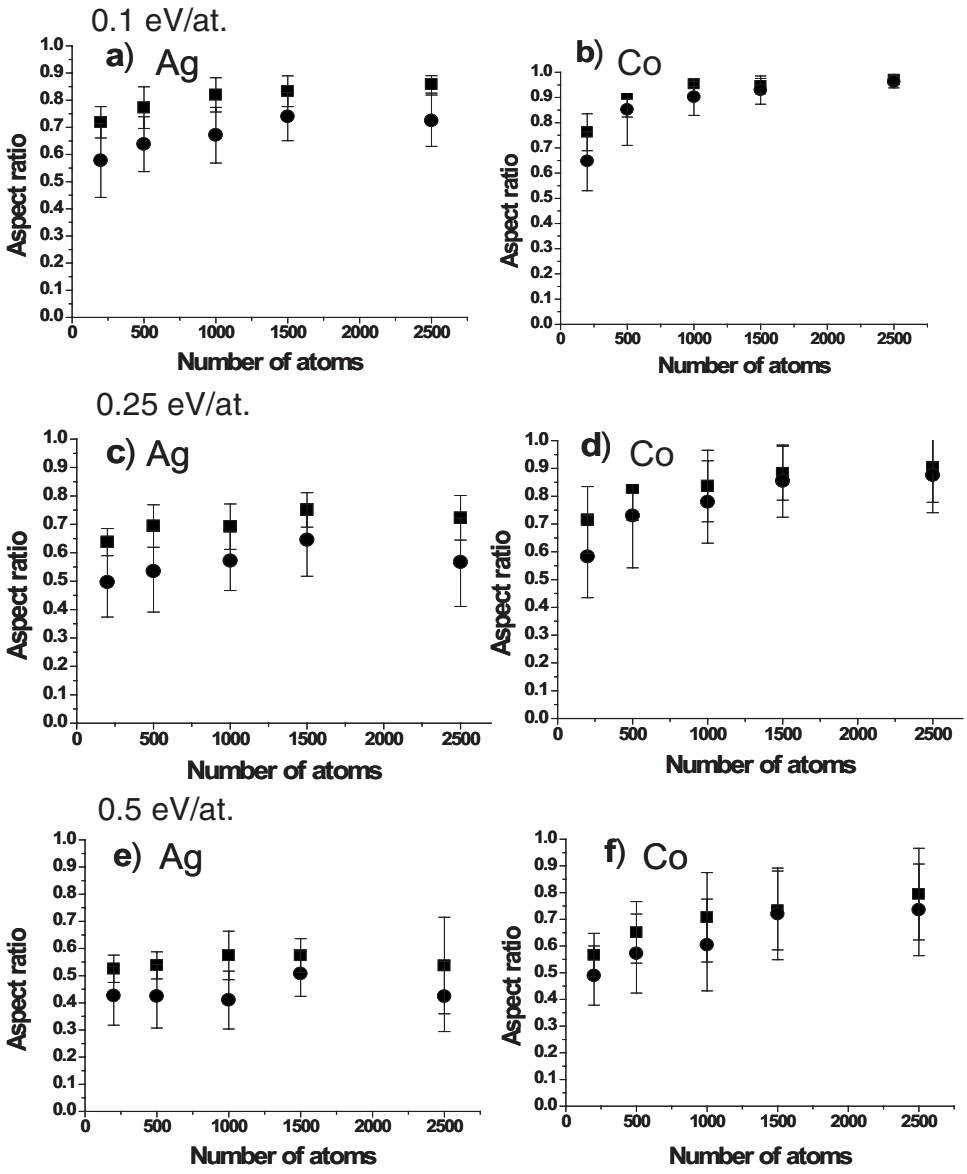

FIG. 7. Aspect ratio and the standard deviation of its distribution (vertical bars) versus cluster size. Results for Ag and Co are given separately in the three nanolayers. Squares: just after deposition of the clusters; circles: after deposition of 70 clusters. Clusters containing 2000, 2500, and 3000 are few and the results concerning them are cumulated and represented with size 2500.

to a tensile stress which balances the excess pressure on Ag. Although smaller than in Ni_3Al samples, the standard deviations of the pressure distributions are quite significant, namely, 2.7 GPa in the Ag system and, somewhat less, 2.2 GPa in the Co system, attesting, as in Ni_3Al, a highly inhomogeneous stress distribution in the material. These inhomogeneities decrease when the temperature is increased but remain of the same order up to the melting temperature.

B. Mechanical response to an external stress

The elastic limit, the plastic behavior, and the yield stress of polycrystalline metals are well known to be governed by the interaction between dislocations and defects such as precipitates and grain boundaries. The dislocation activity and multiplication is, however, dependent on the grain size and becomes insignificant when it is reduced to the nanoscale[34,35,71] at which intragranular deformation mechanisms are inhibited by the limited room available. Because interfaces are disordered and thereby lack periodicity, and because of the limited range of nondestructive characterization techniques, the evolution of intergranular areas is hardly followed experimentally. Therefore, computer modeling represents a useful approach and understanding gathered this way about mechanisms involved is reviewed in Refs. 10 and 72. The MD method described in Sec. III for large plastic deformations is used in what follows.

C. Ni_3Al alloy nanostructures

In Ref. 13 we discussed the mechanical response of cluster assembled Ni_3Al to a uniaxial tensile stress in the case of deformations of limited amplitude (less then 10%). The samples were found to display well distinct elastic and plastic deformation regimes with a yield strength sensitive to the morphology and to the temperature.

Dislocation activity was found during loading, even in grains as small as 2 nm diameter. However, in contrast with the deformation mechanism observed in model single crystal nanowires[73] and consistently with experimental observations

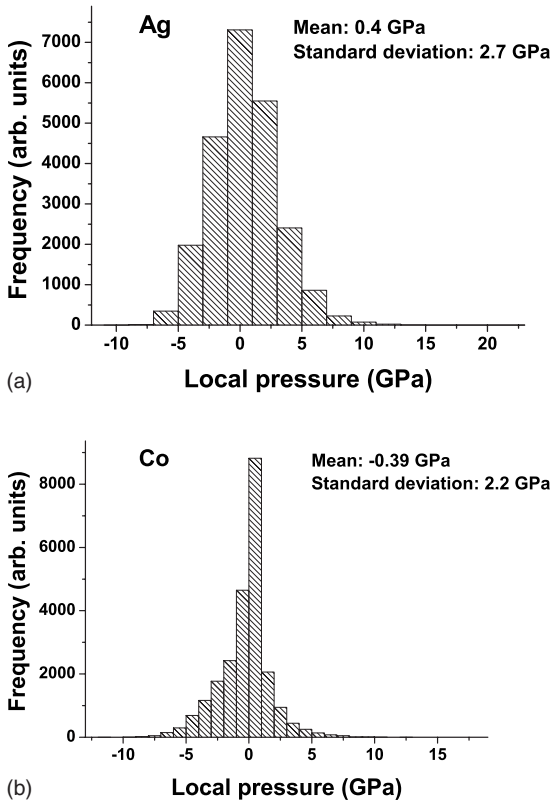

FIG. 8. Distribution of local pressures in the AgCo system. (a) Ag; (b) Co.

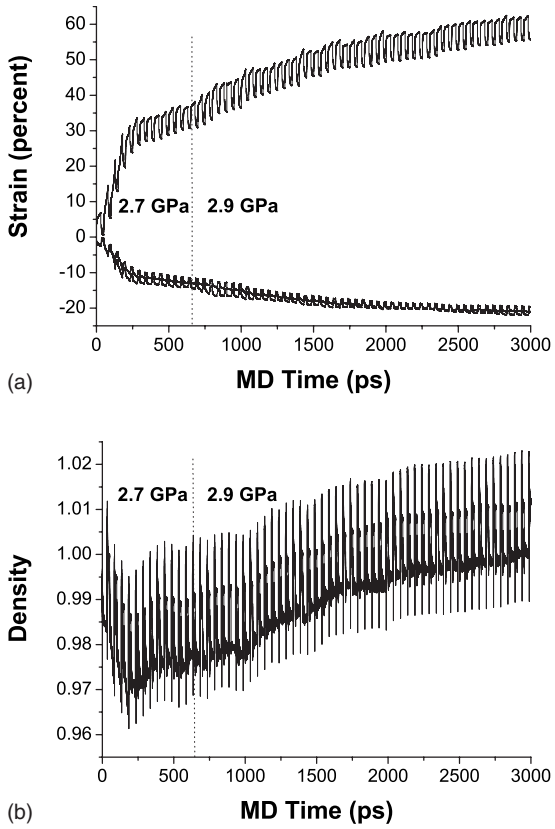

FIG. 9. Series of 60 deformation cycles of the Ni_3Al sample. The load is 2.7 GPa during the first 13 cycles and it is then increased to 2.9 GPa for the next ones. (a) Strain versus the MD time. (b) Density versus MD time.

in bulk nanocrystalline Ni,[3] this limited activity is of minor contribution to the plastic deformation. In the CAM sample used in Fig. 2, open volumes of the same size as the grains are present and are permanently increased by the uniaxial stress. The effect of one load and relaxation cycle on such open volumes is illustrated in Fig. 2(b) showing the evolution of the sample density during the same cycle. The decrease of density illustrates the enlargement of open volumes as a result of the load, without crack nucleation. The enlarged open volumes partially reduce during the relaxation steps with a net reduction of the internal surface energy, thereby stabilizing the nanostructure. This represents the main initial short term plastic deformation mechanism of a cluster assembled Ni_3Al nanoalloy. At the end of one cycle, only part of the strain induced by the load on the whole sample is released. This mechanism differs from model predictions in nanocrystalline Ni with grains separated by planar interfaces and with sizes larger than 5 nm. In the latter nanostructure model, the interfaces contained open volumes limited to a few vacancies only.[10] This difference emphasizes the importance of the nanostructure on the mechanical behavior of nanocrystalline metals. The cycle shown in Fig. 2 may be repeated a number of times and plastic strain accumulates sequentially, as shown in Fig. 9.

The positive strain in the direction of the load is partly balanced by negative strain in orthogonal directions. In the few first cycles, stress induces the enlargement of open volumes, still without initiating cracks, as described above. During the next cycles, however, the deformation induced by the applied stress levels off. This demonstrates that the induced deformation has become elastic and, consequently, the equilibrium density becomes constant. The plastic deformation resulting from the load thus induces an enhancement of the yield strength of the material.

The question now arises to know how far further plastic deformation can be induced by larger stress and if a ductile regime still occurs. In order to answer this question, further deformation cycles were performed with a load increased to 2.9 GPa and the results are also shown in Fig. 9. Further subsequent increase of strain is found but this time, it correlates with an increase of the sample density. The deformation mechanism is thus modified. In this regime, open volumes decrease as a consequence of grain sliding as first identified in Ref. 74 for cluster assembled copper and then confirmed in Ref. 8 for nanostructured Ni modeled by Voronoi construction. During the whole deformation process, the structural evolution of the sample was followed by means of pair distribution functions measured distinctly for the Ni and the Al sublattices (not shown in the figure). No pdf change is found for the Ni system but some was detected in the Al subsystem corresponding to a partial recovery of the $L1_2$ structure, initially deteriorated by the cluster assembling procedure. At the end of the 60 applied deformation cycles, the sample is elongated by 50% and strain levels off again. This time, the yield strength reaches a maximal value. Figure 10 shows the strain versus time applied to the deformed sample, induced by a stress ranging from 2.8 to 3.2 GPa. The in-

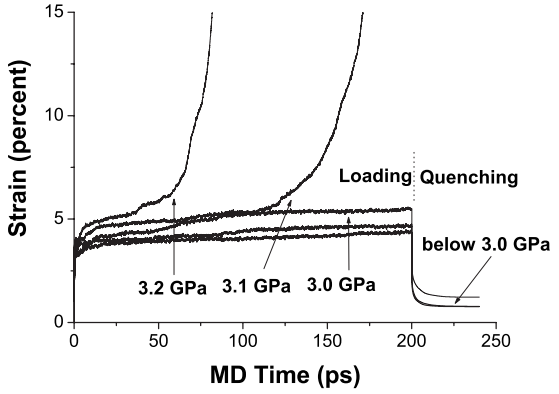

FIG. 10. Time dependence of strain of the Ni_3Al after 60 deformation cycles under uniaxial stresses of different magnitudes. The strain is computed versus the MD time for loads from 2.8 to 3.2 GPa at 300 K applied on the sample at the end of the 60 deformation cycles described in Fig. 13.

crease of yield strength is confirmed around 3.0 GPa.

Open volumes in the nanostructure were stabilized by the former 60 deformation-relaxation cycles. At higher load, the strain rate diverges and the ductile regime vanishes, consistently with the fact that grains are too small for allowing an efficient dislocation activity.

D. AgCo core-shell nanostructures

Plasticity of metallic glasses was recently rationalized, using a continuum theory.[75] Plastic flow was also shown, using atomic scale approaches to be characterized by homogeneous and localized deformations.[76–79] These, however, involve distances well above the nanometer scale to which the system in our model samples is confined. Its layered structure and the presence of the Co grains also represent a difference with metallic glasses, justifying a specific study to which we now proceed.

Qualitatively, the macroscopic mechanical response of AgCo CAM to a constant uniaxial load displays some limited similarity to that of Ni_3Al. Using similar simulations as shown for Ni_3Al in Fig. 1 and restricting ourselves to the constant strain rate regime, a yield strength is indeed identified, which depends on both the nanostructure and the temperature. This comes out in Fig. 11 showing the strain rate as a function of the uniaxial load applied. The results are shown at 0 K, as measured in the samples obtained by deposition at 0.1, 0.25, and 0.5 eV/at. and in the case of the sample synthesized by 0.25 eV/at. deposition, as measured at temperatures of 0, 300, and 600 K. It comes out that the yield strength increases with the material density and decreases with the temperature. Such a temperature dependence was also found in the case of Ni_3Al CAM, featuring a yield strength about twice higher.

The AgCo sample structure largely differs from Ni_3Al because of the core-shell nature of the clusters. In particular, the noncrystalline state of the Ag system, which remains after deposition, may be expected to play a particular role in the plastic deformation of the material. In order to capture the deformation mechanisms involved, similar series of de-

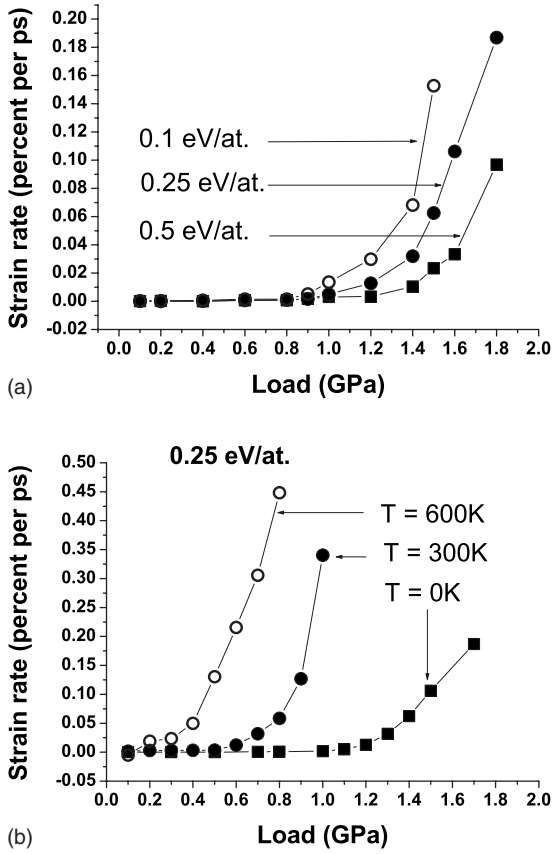

FIG. 11. Strain rate as a function of the magnitude of a uniaxial stress applied to the AgCo material assembled by cluster deposition. (a) Response at 0 K of the samples obtained with different deposition energies. (b) Response of the sample obtained with 0.25 eV/at. at different temperatures.

formation cycles as presented in Sec. VI B in the case of Ni_3Al are achieved with the samples built with 0.25 and 0.5 eV/at. AgCo cluster deposition. In what follows, for convenience, they will be named the 0.25 eV/at. and 0.5 eV/at. samples, respectively. Illustrative cases are depicted in Fig. 12. A common morphological feature to the 0.25 eV/at. sample and the Ni_3Al one is the occurrence of large open volumes between clusters. The deformation mechanism is, however, opposite. Indeed, instead of enlarging, open volumes in AgCo shrink with the consequence of increasing the material density. This is shown in Fig. 12(b) in the case of a deformation by a 0.9 GPa uniaxial stress at 300 K. When shrinkage is achieved, after about 10 cycles, the applied stress becomes insufficient to induce any further plastic deformation and the deformation induced by the next cycles at 0.9 GPa is elastic. In this case, the improvement of the elastic properties is thus the consequence of the disappearance of open volumes. After 20 cycles with 0.9 GPa load, a new series of 30 cycles at 1.2 GPa was performed. As it comes out from Figs. 12(a) and 12(b), and again in contrast with the case of Ni_3Al, further plastic deformation proceeds with no change in the density of the sample, indicating that this deformation may induce no structural change in the sample. A similar behavior is found in the 0.5 eV/at. sample. Figures 12(c) and 12(d) depict its deformation at 300 K using a

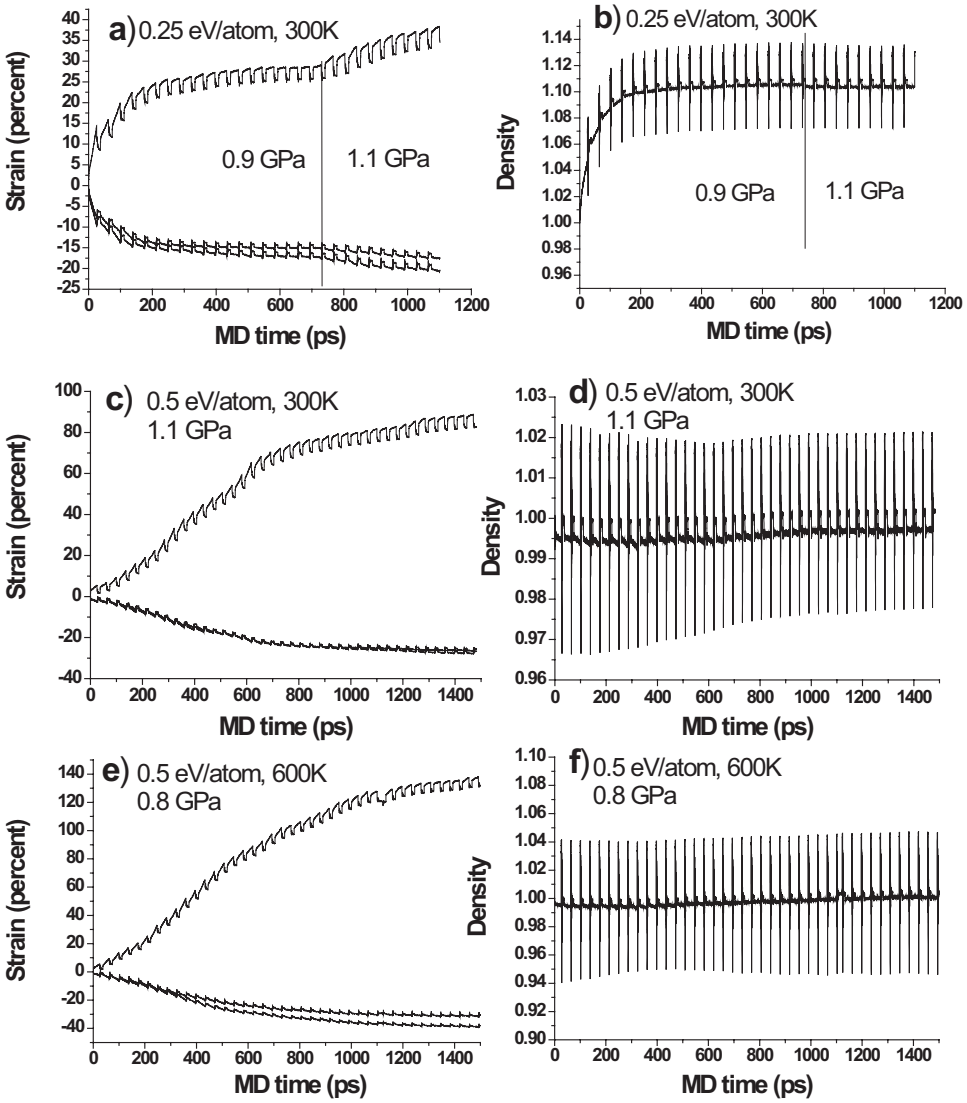

FIG. 12. Series of deformation cycles of the CoAg core-shell sample, similar to that described in Fig. 12. The evolutions of strain as well as the sample densities with the MD evolution time are represented; (a),(b) at 300 K, of the sample synthesized with 0.25 eV/atom deposition energy subjected to 20 deformation cycles with 0.9 GPa followed by 30 cycles with 1.2 GPa load; (c),(d) at 300 K, of the sample synthesized with 0.5 eV/atom deposition energy subjected to 40 cycles with 1.1 GPa load; and (e), (f) at 600 K, of the sample synthesized with 0.5 eV/atom deposition energy subjected to 40 cycles with 0.8 GPa load.

1.1 GPa load in forty cycles. In this case, a total plastic strain of 80% is reached. Since the sample displays no open volume before deformation, the density remains constant since the first cycle. In this respect, the mechanical response of the 0.5 eV/at. sample is the same as that of the 0.25 eV/at. sample. However, the slope of the strain dependence decreases as the number of cycles increases. This indicates a progressive change in the sample morphology, which will be discussed on the example of the deformation depicted in Figs. 12(e) and 12(f). Strain is here induced in the same 0.5 eV/at. sample with a lower load, 0.8 GPa, but at a higher temperature, 600 K. Increasing temperature not only results in lowering the yield strength, but also facilitates the plastic deformation. Close to 140% strain was obtained with forty deformation cycles and, again, this deformation induces no change in the density. Again, the overall strain is no linear function of the number of deformation cycles which is the signature of the modification of the mechanical properties and thus of a stress induced modification of the sample structure. It is a slab of this sample which is displayed in Fig. 13, before and after the deformation cycles depicted in Figs. 12(e) and 12(f). The deformation is superplastic, however, as in the previous cases depicted, the yield strength is increased. The deformation modifies neither the sample density nor its structure, as will now be discussed. Although the packing of clusters into a material slightly modifies their morphologies, it is found in Fig. 13 that their core-shell structure is preserved. The Co grains appear as embedded into a Ag matrix where the interfaces between neighbor clusters have vanished.

The pdfs of Co and Ag in a 3000 atom cluster are compared before and after the superplastic deformation in Fig. 14. Both display the same features as in the clusters before deposition, showing that structural properties are not altered by deposition nor by the deformation. The evolution of the Co subsystem is not fully captured by the analysis of the pair distribution functions. Indeed, as it comes out in Fig. 13, the huge deformation of the sample modifies the spatial distribution of the Co clusters in the Ag matrix and Co cluster coalescence takes place. This is illustrated by Fig. 15 showing the evolution with the MD time (or the number of deformation cycles) of the number of first neighbor bonds between Co atoms of initially different clusters, which correlates with the magnitude of the strain [Fig. 12(a)]. Since neither the

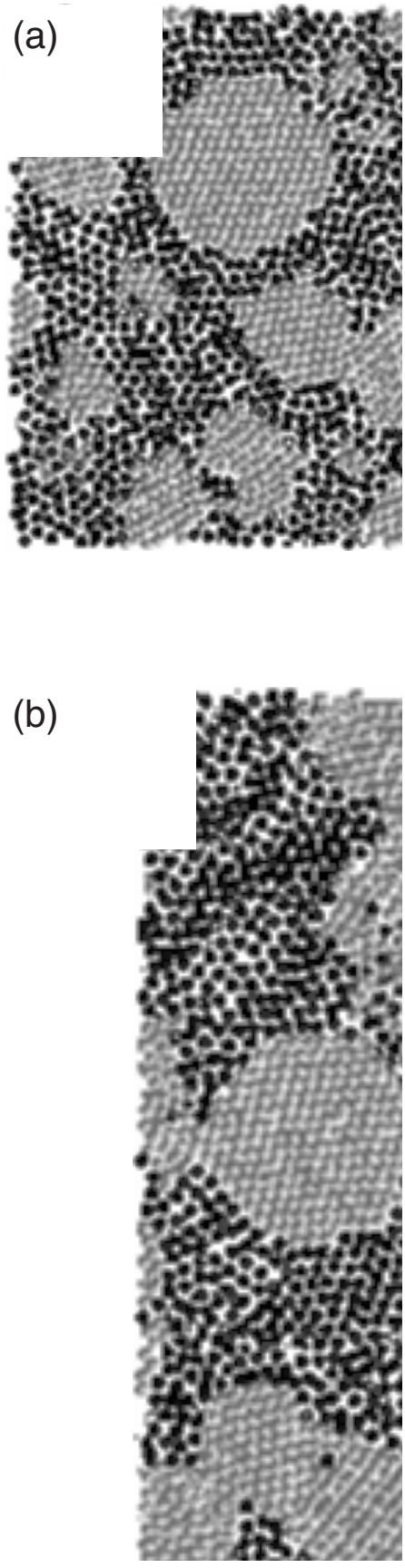

FIG. 13. One slab in a AgCo nanostructured box, before (a) and after (b) deformation at 600 K with a uniaxial load of 0.8 GPa.

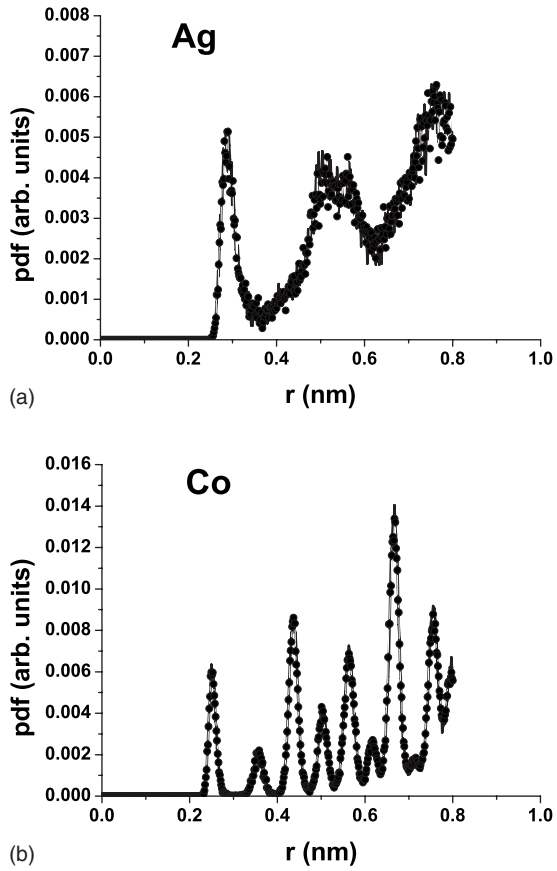

FIG. 14. Pair distribution functions in the Ag shell (a) and in Co core (b) of a 3000 atom cluster embedded in a cluster assembled layer containing 80 clusters. The deposition energy is 0.25 eV/at. The solid lines show the pdfs before deformation and the dots show the pdfs after deformation with a uniaxial load of 0.9 GPa for 100 ps. The deformation induces no significant modifications in the pdfs that are also most similar to those in the same cluster before deposition, as shown in Fig. 1.

sample density nor the Co crystallinity is affected by the superplastic deformation, coalescence is the only process identified at this stage, giving rise to the improvement of the elastic properties. As shown next, it may also be the process limiting superplasticity, beyond the presently computed deformation amplitudes.

In order to get a full picture of the sample deformation, it is useful to appreciate the deformations of the Ag and of the Co subsystems independently. To this purpose, cluster morphologies are examined in terms of their aspect ratio. Although no grain boundaries separate the Ag shells, this procedure helps to figure out the deformations. The results are summarized for one of the deformed AgCo samples in Fig. 16 and they are representative of the others. Their broad distributions demonstrate large inhomogeneities, already taking place in the initial configurations. The sample preparation is thus responsible therefore. The contribution of deformation is to steer the Ag shells in the direction of the applied load much more than Co cores. The picture which comes out is thus the crystalline Co grains, embedded in a layered noncrystalline Ag system acting as a viscous medium. The resulting shear stress on the Co grains is high enough to induce

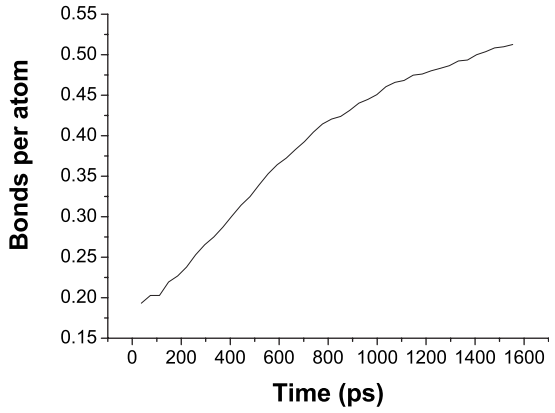

FIG. 15. Evolution with the MD time of the coalescence of the Co cores. The fraction of first neighbor bonds per atom is represented as a function of the MD time between Co atoms belonging to different grains.

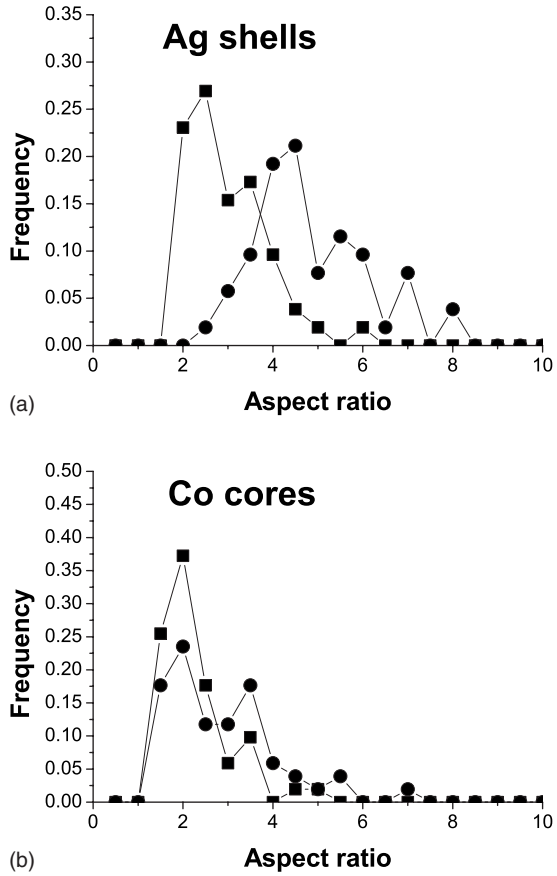

FIG. 16. Cluster shape distributions. Distributions of the aspect ratios are represented before (squares) and after (circles) 60 cycles deformation of the CAM AgCo sample. (a) Silver shells; (b) Co cores.

their elongation, however, with smaller amplitude than the steering of Ag. Since the elongation of the sample proceeds at constant volume, its cross section decreases. The consequence is a decrease of the separation between the Co cores and, as comes out in Fig. 15, solid state coalescence is induced, caused by the morphological evolution. The physical limit to Co clusters steering and coalescence is the total material phase separation. This may also represent a limit to the superplastic behavior. Another possible physical limit is the propagation of defects nucleated at the surface of real samples, which could be accounted for in simulations similar to those presented here. Even at surfaces, however, because of the limited grain size and although dislocations might nucleate, their multiplication is not expected, neither the propagation of cracks.

VII. CONCLUSION

In this work, clusters, considered as the building blocks of cluster assembled materials, are studied first, their assembling next, and then the properties of the cluster assemblies. Two different bimetallic systems are considered. Ni_3Al alloy clusters display the same structure as the bulk material. Surface segregation may occur, but is predicted to be at most of the order of 10%.[36] Full segregation takes place in AgCo clusters,[47] Ag and Co being no miscible elements in the bulk. In small clusters—containing typically less then 5000 atoms—the Ag shell is not crystalline but it displays a layered structure induced by the crystalline Co cores.

When deposited on a surface at supersonic velocities (a fraction of an eV/atom), both the Ni_3Al and the CoAg clusters keep their structural properties. When accumulated on a substrate, Ni_3Al clusters form a nanostructured layer in which the clusters keep their identity. The cluster stacking resembles a stacking of hard balls in which open volumes and pores have characteristic sizes similar to the cluster sizes themselves.[38] AgCo core-shell materials are here predicted with peculiar properties but, to our knowledge, they are not yet synthesized. Since the Ag shells are noncrystalline, they are easily deformed and, depending upon the slowing down energy, they may form a nanoporous medium or a compact one. Ni_3Al and AgCo materials have thus different morphologies and structures, and this has an impact on their mechanical properties.

The stress distribution in both is highly inhomogeneous. However, because of their larger hardness, Ni_3Al clusters do not accommodate much with each other during deposition and the stress distribution in Ni_3Al cluster assemblies is subsequently broader and has a higher mean value than in AgCo cluster assemblies. One consequence is that, when subjected to a uniaxial external stress, Ni_3Al clusters still do not accommodate and the main kernel for plastic deformation is the enlargement of the open volumes. Intergranular atomic diffusion in the long term, neglected in the present approach, may moderate this effect. This enlargement is limited, however, and, in the case of large deformations, they partially shrink, making the material denser. When available, open volumes in AgCo cluster assemblies are unstable and they start to shrink as soon as an external uniaxial stress is applied. When the material is deformed further, the layered structure of the Ag system remains unchanged and the density of the material remains constant. The Co cores only undergo little deformation. Since deforming the material induces no structural evolution, its deformation is superplastic. This contrasts with the case of Ni_3Al where the shrinkage of

open volumes can only be limited and, beyond this limit, the material is embrittled. Again, atomic diffusion in the long term may moderate the embrittlement.

In both Ni_3Al and AgCo cluster assemblies, the effect of applying an external stress is to improve the elastic properties. This is consistent with the stabilization of the open volumes in Ni_3Al and with the mechanically induced coalescence of Co clusters in AgCo. This coalescence is also anticipated to be a limiting factor to the superplastic behavior of AgCo cluster assemblies.

The effect of temperature on mechanical properties was investigated as well. For both materials, the yield strength is found to be quite sensitive to the temperature, particularly in the range of room temperature. This suggests the possibility to design materials in which type of response to an external stress can be monitored. In the plastic regime, the deformation mechanisms are not found to be significantly temperature dependent in the range investigated (0–600 K). They may be anticipated, however, to change in the case of AgCo at more elevated temperature. Indeed, it was found in Ref. 47 that AgCo free clusters may exist at thermodynamic equilibrium with a solid Co core and a liquid Ag shell. In cluster assemblies, it thus may be anticipated that, at such temperatures, the material would behave as an ordinary viscous fluid carrying solid grains.

In the present study, the role of surfaces in the deformation mechanisms of nanostructured materials is still not considered but deserves deep interest as surfaces are known to be a source of migrating defects. One example is dislocations in which nucleation and propagation could explain some mechanical properties of crystalline nanowires.[80] The propagation of dislocations in materials formed by nanoclusters is inhibited, and should not contribute much to the deformation of nanowires if the cluster size is smaller than the wire diameter. To our knowledge, such cluster assembled wires are not available yet but the routes for synthesizing them probably exist. Their modeling study is under way.

ACKNOWLEDGMENTS

E.Z. is thankful to the "Fonds National de la Recherche Scientifique" of Belgium (F.N.R.S.) and T.V. to the "Fonds de la Recherche pour l'Industrie et l'Agriculture" of Belgium (F.R.I.A.) for allotted grants. The research was achieved within the agreement 2.4520.03F with the "Fonds National de la Recherche Collective" of Belgium (F.R.F.C.) and relates to the Belgian cooperation network IAP 5-10 "Quantum size effects in nanostructured materials."

*Email address: mhou@ulb.ac.be

[1] E. Q. Hall, Proc. Phys. Soc. London, Sect. B **64**, 747 (1951).
[2] N. J. Petch, J. Iron Steel Inst., London **174**, 25 (1953).
[3] Z. Budrovic, H. Van Swygenhoven, P. M. Derlet, S. Van Petegem, and B. Schmitt, Science **304**, 273 (2004).
[4] R. Z. Valiev, Mater. Sci. Forum **243-244**, 207 (1997).
[5] V. Yamakov, D. Wolf, D. W. S. R. Philipot, A. K. Mukherjee, and H. Gleiter, Nat. Mater. **1**, 45 (2002).
[6] V. Yamakov, D. Wolf, D. W. S. R. Philipot, A. K. Mukherjee, and H. Gleiter, Nat. Mater. **3**, 43 (2004).
[7] J. Schiøtt, F. D. Di Tolla, and K. W. Jacobsen, Nature (London) **393**, 561 (1998).
[8] H. Van Swygenhoven and A. Caro, Appl. Phys. Lett. **71**, 1652 (1997).
[9] P. M. Derlet, H. Van Swygenhoven, and A. Hasnaoui, Philos. Mag. **83**, 3569 (2003).
[10] H. Van Swygenhoven and J. R. Weertman, Mater. Today **9**, 24 (2006).
[11] D. Farkas, H. Van Swygenhoven, and P. M. Derlet, Phys. Rev. B **66**, 060101(R) (2002).
[12] A. Latapie and D. Farkas, Modell. Simul. Mater. Sci. Eng. **11**, 745 (2003).
[13] E. E. Zhurkin, G. Hautier, and M. Hou, Phys. Rev. B **73**, 094108 (2006).
[14] A. P. Sutton and R. W. Baluffi, *Interfaces in Crystalline Materials* (Oxford Scientific, Oxford, UK, 1995).
[15] Q. Hou, M. Hou, L. Bardotti, B. Prével, P. Mélinon, and A. Perez, Phys. Rev. B **62**, 2825 (2000).
[16] H. Van Swygenhoven, M. Spaczer, and A. Caro, Acta Mater. **47**, 3117 (1999).
[17] H. Haberland, Z. Insepov, and M. Moseler, Phys. Rev. B **51**, 11061 (1995).
[18] L. Bardotti, B. Prével, P. Mélinon, A. Perez, Q. Hou, and M. Hou, Phys. Rev. B **62**, 2835 (2000).
[19] H. Haberland, *Clusters of Atoms and Molecules* (Springer-Verlag, Berlin, 1995).
[20] K. H. Meiwes-Broer, *Clusters on Surfaces* (Springer-Verlag, Berlin, 2000).
[21] L. W. Zhong, L. Yi, and S. Ze, *Handbook of Nanophase and Nanostructured Materials* (Kluwer Academic, New York, 2003).
[22] T. Van Hoof and M. Hou, Phys. Rev. B **72**, 115434 (2005).
[23] M. Schmidt and H. Haberland, C. R. Phys. **3**, 327 (2002).
[24] T. P. Martin, Phys. Rep. **273**, 199 (1996).
[25] S. Neukermans, E. Janssens, H. Tanaka, R. E. Silverans, and P. Lievens, Phys. Rev. Lett. **90**, 033401 (2003).
[26] B. Pauwels, G. Van Tendeloo, W. Bouwen, L. Theil Kuhn, P. Lievens, H. Lei, and M. Hou, Phys. Rev. B **62**, 10383 (2000).
[27] B. Pauwels, G. Van Tendeloo, E. E. Zhurkin, M. Hou, G. Verschoren, L. Theil Kuhn, W. Bouwen, and P. Lievens, Phys. Rev. B **63**, 165406 (2001).
[28] C. L. Cleveland, W. D. Luedtke, and U. Landman, Phys. Rev. Lett. **81**, 2036 (1998).
[29] C. L. Cleveland, W. D. Luedtke, and U. Landman, Phys. Rev. B **60**, 5065 (1999).
[30] H. A. Dürr, S. S. Dhesi, E. Dudzik, D. Knabben, G. van der Laan, J. B. Goedkoop, and F. U. Hillebrecht, Phys. Rev. B **59**, R701 (1999).
[31] R. Röhlsberger, J. Bansmann, V. Senz, K. L. Jonas, A. Bettac, O. Leupold, R. Rüffer, E. Burkel, and K. H. Meiwes-Broer, Phys. Rev. Lett. **86**, 5597 (2001).
[32] P. Mélinon, V. Paillard, V. Dupuis, A. Perez, P. Jensen, A. Hoareau, J. P. Perez, J. Tuaillon, M. Broyer, J.-L. Viale, M. Pélarin,

B. Baguenard, and J. Lermé, Int. J. Mod. Phys. B **39**, 339 (1995).
[33] J. Bansmann, S. H. Baker, C. Binns, J. A. Blackman, J.-P. Bucher, J. Dorantes-Dàvila, V. Dupuis, A. Kleibert, K. H. Meiwes-Broer, G. M. Pastor, A. Perez, O. Toutlemonde, K. N. Trohidou, J. Tuaillon, and Y. Xie, Surf. Sci. Rep. **56**, 189 (2005).
[34] H. Gleiter, Prog. Mater. Sci. **33**, 1 (1989).
[35] J. R. Weertman, Mater. Sci. Eng., A **166**, 161 (1993).
[36] E. E. Zhurkin and M. Hou, J. Phys.: Condens. Matter **12**, 6735 (2000).
[37] V. S. Kharlamov, E. E. Zhurkin, and M. Hou, Nucl. Instrum. Methods Phys. Res. B **193**, 538 (2002).
[38] M. Hou, V. S. Kharlamov, and E. E. Zhurkin, Phys. Rev. B **66**, 195408 (2002).
[39] E. E. Zhurkin and M. Hou, J. Alloys Compd. (to be published).
[40] R. Meyer, S. Prakash, and P. Entel, Phase Transitions **75**, 51 (2002).
[41] L. Favre, S. Stanescu, V. Dupuis, E. Bernstein, T. Epicier, P. Mélinon, and A. Perez, Appl. Surf. Sci. **226**, 256 (2004).
[42] E. Janssens, T. Van Hoof, N. Veleman, S. Neukermans, M. Hou, and P. Lievens, Int. J. Mass. Spectrom. **252**, 38 (2006).
[43] M. Gaudry, E. Cottancin, M. Pellarin, J. Lermé, L. Arnaud, J. R. Huntzinger, J. L. Vialle, M. Broyer, J. L. Rousset, M. Treilleux, and P. Mélinon, Phys. Rev. B **67**, 155409 (2003).
[44] G. Rossi, A. Rapallo, C. Mottet, A. Fortunelli, F. Baletto, and R. Ferrando, Phys. Rev. Lett. **93**, 105503 (2004).
[45] F. Baletto, C. Mottet, and R. Ferrando, Eur. Phys. J. D **24**, 233 (2003).
[46] A. Rapallo, G. Rossi, R. Ferrando, A. Fortunelli, B. C. Curley, L. D. Loyd, G. M. Tarbuck, and R. L. Johnston, J. Chem. Phys. **92**, 194308 (2005).
[47] T. Van Hoof and M. Hou, Phys. Rev. B **72**, 115434 (2005).
[48] A. Dzhurakhalov, A. Rasulov, T. Van Hoof, and M. Hou, Eur. Phys. J. D **31**, 53 (2004).
[49] T. Van Hoof, A. Dzhurakhalov, and M. Hou, Eur. Phys. J. D (to be published).
[50] F. Ducastelle, J. Phys. (France) **31**, 133 (1970).
[51] M. W. Finnis and J. E. Synclair, Philos. Mag. A **50**, 45 (1984).
[52] G. J. Ackland and V. Vitek, Mater. Res. Soc. Symp. Proc. **133**, 105 (1989).
[53] G. J. Ackland and V. Vitek, Phys. Rev. B **41**, 10324 (1990).
[54] F. Gao, D. Bacon, and G. Ackland, Philos. Mag. A **67**, 275 (1993).
[55] M. S. Daw and M. I. Baskes, Phys. Rev. Lett. **50**, 1285 (1983).
[56] R. A. Johnson, Phys. Rev. B **39**, 12554 (1989).
[57] R. A. Johnson, Phys. Rev. B **41**, 9717 (1990).
[58] M. Hou, M. El Azzaoui, H. Pattyn, J. Verheyden, G. Koops, and G. Zhang, Phys. Rev. B **62**, 5117 (2000).
[59] M. P. Allen and D. Tildesley, *Computer Simulation of Liquid* (Clarendon Press, Oxford, 1987).
[60] M. Parrinello and A. Rahman, Phys. Rev. Lett. **45**, 1196 (1980).
[61] M. Parrinello and A. Rahman, J. Appl. Phys. **52**, 7182 (1981).
[62] S. Nosé, J. Chem. Phys. **81**, 511 (1984).
[63] M. W. Finnis, P. Agnew, and A. J. E. Foreman, Phys. Rev. B **44**, 567 (1991).
[64] P. S. Branicio and J.-P. Rino, Phys. Rev. B **62**, 16950 (2000).
[65] A. F. Voter, Phys. Rev. Lett. **78**, 3908 (1997).
[66] M. R. Sørensen and A. F. Voter, J. Chem. Phys. **112**, 9599 (2000).
[67] G. M. Torrie and J. P. Valleau, J. Comput. Phys. **23**, 187 (1977).
[68] M. Hou, Phys. Rev. B **31**, 4178 (1985).
[69] R. A. Salkar, P. Jeevanandam, S. T. Aruna, Y. Koltypin, and A. Gedanken, J. Mater. Chem. **9**, 1333 (1999).
[70] J. Tuaillon-Combes, O. Boisron, E. Bernstein, A. Gerbert, A. Milner, P. Mélinon, and A. Perez, Appl. Surf. Sci. **226**, 321 (2004).
[71] R. Z. Valiev, N. K. Tsenev, D. A. Salimonenko, P. Berbon, and T. G. Longdon, Scr. Mater. **37**, 1945 (1997).
[72] K. W. Jacobsen and J. Schiøtt, Nat. Mater. **1**, 15 (2002).
[73] S. J. A. Koh, H. P. Lee, C. Lu, and Q. H. Cheng, Phys. Rev. B **72**, 085414 (2005).
[74] H. Zhu and R. S. Averback, Mater. Sci. Eng., A **204**, 96 (1995).
[75] S. Braeck and Y. Y. Podladchikov, Phys. Rev. Lett. **98**, 095504 (2007).
[76] M. L. Falk and J. S. Langer, Phys. Rev. E **57**, 7192 (1998).
[77] X.-Y. Fu, D. A. Rigney, and M. L. Falk, J. Non-Cryst. Solids **317**, 206 (2003).
[78] Y. Shi and M. L. Falk, Appl. Phys. Lett. **86**, 011914 (2005).
[79] A. S. Argon and M. J. Demkowicz, Philos. Mag. **86**, 4153 (2006).
[80] M. D. Uchic, D. M. Dimiduk, J. N. Florando, and W. D. Nix, Science **305**, 986 (2004).